

# Young's modulus, hardness and scratch adhesion of Ni–P–W multilayered alloy coatings produced by pulse plating

V.D. Papachristos<sup>a,\*</sup>, C.N. Panagopoulos<sup>a</sup>, L.W. Christoffersen<sup>b</sup>, A. Markaki<sup>c</sup>

<sup>a</sup>Laboratory of Physical Metallurgy, National Technical University of Athens, 157 80 Zografos, Athens, Greece

<sup>b</sup>Department of Manufacturing Engineering, Technical University of Denmark, 2800 Lyngby, Denmark

<sup>c</sup>Department of Materials Science and Metallurgy, University of Cambridge, Cambridge, UK

Received 20 October 2000; received in revised form 8 May 2001; accepted 20 June 2001

## Abstract

The effect of layering on Young's modulus, hardness and deformation behaviour of Ni–P–W multilayered alloy coatings in a scratch adhesion test was studied. The coatings were deposited on copper substrates by electro-deposition and the wavelengths studied were 8–4000 nm. The Young's moduli of the amorphous multilayered Ni–P–W coatings, measured by an acoustic-wave resonance method, are higher than the Young's modulus of crystalline nickel. Their hardness was found to increase with decreasing wavelength of the coatings, the increase being more pronounced for wavelengths below 120 nm. The cohesive load of the multilayered coatings ranges from 5 to 16 N, while the critical load range for coating detachment in scratch adhesion tests was found to be 50–75 N. The values of adhesive and cohesive loads seem to be independent from the wavelength of the Ni–P–W coatings. The failure modes observed in the scratch tracks of the Ni–P–W multilayered coatings are common in every coating in the scratch tests under increasing load, and they are a result of substrate deformation and coating brittleness. © 2001 Elsevier Science B.V. All rights reserved.

**Keywords:** Young's modulus; Adhesion; Hardness; Multilayers

## 1. Introduction

The investigation of the mechanical properties of many metallic multilayered coatings, and the effect that layering may have on them, has attracted the attention of many researchers during the last 20 years and especially during the last decade. The reason is that knowledge of the elastic moduli, hardness and adhesion of a coating is very important for its evaluation in terms of load carrying capacity, necessary in numerous applications.

Since the work of Yang et al. [1], who reported a 120% increase in the [111] biaxial modulus of strongly oriented, vacuum deposited Au/Ni multilayered coat-

ings, comparing to the biaxial modulus of a homogeneous coating of the same composition, a lot of studies have also reported anomalously high values (up to 310% increase), in the elastic moduli of crystalline multilayers with wavelength below 4 nm [2–5]. The above results were initially interpreted by the researchers as a 'supermodulus effect', and various theories based on either the electronic structure of the atoms in the layers or the existence of interface related stresses, were developed in order to explain the elastic anomalies [1–7]. However, later studies disputed the existence of a supermodulus effect [8–13], and finally, new tests in multilayered systems that had been reported to show a supermodulus effect, showed that the first results were erroneous owing to shortcomings of the initial testing procedures [12].

Investigation of the effect of layering on the hardness of metallic multilayered coatings has not resulted in such controversy. It is generally accepted that the hard-

\* Corresponding author. Tel.: +30-1-772-2171; fax: +30-1-772-2119.

E-mail address: vpapachr@metal.ntua.gr (V.D. Papachristos).

ness of crystalline multilayered coatings reaches a maximum value for wavelengths in the range between 2 and 5 nm, while it decreases for both larger and smaller wavelengths [14–20]. At its maximum value, the hardness of the metallic multilayered coatings can be increased up to 100%, compared with the rule of mixture value, estimated using the hardness of the elements consisting of the multilayer.

The decrease in hardness for larger wavelengths has been found to follow the Hall–Petch relationship ( $H = H_0 + k/d^{1/2}$ ), where  $d$  is 1/2 the bilayer thickness,  $H_0$  is the rule of mixture hardness and  $k$  is a constant. According to this approach, the interfaces are considered to act in a similar way as grain boundaries, pilling up the dislocations and thus obstructing their movement. Increased plastic resistance (i.e. hardness) of crystalline multilayered coatings is also expected by the Kohler theory [21], since a sequence of layers with different elastic constants obstructs dislocation movement between the layers, whereas the small layer thickness blocks the dislocation sources.

The decrease in hardness for smaller wavelengths ( $\lambda < 2$  nm) cannot be explained by Hall–Petch theory, since its validity does not hold for such small wavelengths [22]. Therefore, it was suggested, that in small wavelengths, hardness is controlled by film stresses [17–19], coherency stresses [16], and integrity of layering [20].

Up to now, the adhesion of a few multilayered coatings has been studied, and the majority of them are ceramic or metallic/ceramic [23] multilayers. To the best of our knowledge, the only adhesion study in metallic multilayers comes from Lin et al. [24], who studied the adhesion of multilayered Al/Mo/Ni and Al/Zn/Ni–P coatings on a silicon substrate, with the aid of a pull test.

In the present study, the effect of layering on Young's modulus, hardness and adhesion of an electro-deposited Ni–P–W multilayered coating, consisting of alternate amorphous layers of Ni–P–W ternary alloys with different composition is investigated. Furthermore, using the set up of the scratch test, the deformation behaviour of the coating–substrate system under the tangential movement of the load acting on the surface of the coating is studied.

## 2. Experimental

The Ni–P–W multilayered coatings were deposited on annealed (1 h at 350°C in an inert atmosphere) copper substrates. Prior to the deposition, the substrates were cleaned for 2–5 min in a cathodic degreasing bath (NaCN 15 g/l, Na<sub>2</sub>CO<sub>3</sub> 15 g/l, NaOH 60 g/l, at 25°C, voltage between anode and cathode 3 V, anode: IrO<sub>2</sub> coated Ti), rinsed with water and activated for 10 s in

a bath containing 10% in weight H<sub>2</sub>SO<sub>4</sub> and 100 ml/l H<sub>2</sub>O<sub>2</sub> (35%), at room temperature.

The plating solution had the following composition:

NiSO <sub>4</sub> ·6H <sub>2</sub> O	17 g/l
Na <sub>2</sub> WO <sub>4</sub> ·2H <sub>2</sub> O	66 g/l
H <sub>3</sub> PO <sub>3</sub>	25 g/l
Citric acid monohydrate	63 g/l
pH	5.5
Temperature	70°C
Anodes	IrO <sub>2</sub> coated Ti or AISI 316 stainless steel

From this solution, amorphous alternate Ni–P–W layers of low and high tungsten content were deposited. The average composition of the layers was Ni–8%P–15%W and Ni–5%P–45%W in weight (Ni–16%P–5%W and Ni–13%P–19%W at.%), for the low and high tungsten layers, respectively. The thickness ratio of the multilayered Ni–P–W coatings was one-quarter of the wavelength thickness for the low-W layer and three-quarters of the wavelength thickness for the high-W layer. The amorphous nature of the alternate layers was shown by transmission electron microscope (TEM) images, X-ray diffraction (XRD) and selected area electron diffraction (SAED) patterns, while the composition of the layers was measured by EDS on cross-sections of the coatings, in a transmission electron microscope. More details on the structure of the amorphous Ni–P–W coatings can be found elsewhere [25].

The low tungsten content layer was deposited during the low current density step of the cathodic pulse which was 20 mA/cm<sup>2</sup>, whereas the high tungsten content layer was deposited during the high current density step of the cathodic pulse, which was 200 mA/cm<sup>2</sup>. Both pulses were followed by an anodic pulse with an anodic-to-cathodic charge ratio  $q_a/q_c$  3.6 and 3.2%, respectively. Each layer was deposited with the use of its own basic waveform (cathodic pulse followed by the anodic pulse), which was repeated 1–500 times, until the desired layer thickness had been reached. The high-W layer was always on the top.

For the measurement of Young's modulus, the Ni–P–W coatings were deposited on both sides of 30 × 10 × 0.6 mm<sup>3</sup> copper sheets. The wavelengths (bilayer thickness) of the multilayered coatings were 8, 16, 40, 400 and 4000 nm and their total thickness (on each side) 39–46 μm.

An acoustic-wave resonance method was used for the measurement of Young's modulus. The specimens were suspended from two elastic nodes placed at distances 0.224*L* from their edges (where *L* is the length of the specimen), while they were also supported by a plastic bar at their midpoint. The specimens were set into flexural oscillation by an acoustic drive at their middle, for a range of acoustic frequencies. A transducer placed in the plastic bar at the middle of the specimens and in contact with them, recorded the resonant frequencies and the dominant resonant frequency *f* (in Hz) was

given by a Grindosonic Mk5 frequency analyser. The plane strain modulus can then be estimated from the following equation:

$$E^* = 0.94642 \frac{\rho L^4 f^2 \Gamma}{h^2} \quad (1)$$

where  $\rho$  is the density of the specimens in  $\text{kg}/\text{m}^3$  (estimated by weighing and precise measurement of the specimens' dimensions),  $L$  and  $h$  the length and the thickness of the specimens in meters, respectively, and  $f$  the dominant resonant frequency in Hz.  $\Gamma$  is a dimensionless shape factor that can be ignored for the length-to-thickness ratio of the sample  $> 30$  (in our case 50).

For the calculation of Young's modulus of the Ni–P–W multilayered coatings, the plane strain modulus of each copper substrate  $E^*$ , and the composite plane strain modulus of the same substrate, coated with the multilayered coating  $E^*_{\text{comp}}$  was measured. Then, the flexural rigidity or bending modulus  $D$  was used for the calculation of the plane strain modulus of the multilayered coating  $E^*_c$  (see Appendix A). The Young's modulus of the coating is finally calculated by the following equation [41]:

$$E_c = E^*_c (1 - \nu^2) \quad (2)$$

where  $E_c$  is the Young's modulus of the coating and  $\nu$  the Poisson ratio (taken as 0.3 in this study). Each value is the average of at least five measurements.

For hardness measurements, the multilayered coatings were deposited on 200- $\mu\text{m}$ -thick copper foils, using a rotating cylinder electrode. Their wavelengths were 8, 12, 16, 40, 120, 400, 1200 and 4000 nm, and their total thickness was approximately 25  $\mu\text{m}$ . A Shimadzu HMV 2000 microhardness tester was used for the indentations, which were carried out on the surface of the coatings. A Vickers indenter was used and the applied load was 25 g for 15 s. For the selected load, any substrate effects on hardness were avoided, since the maximum indentation depth (1.57  $\mu\text{m}$ ) was smaller than one-tenth of the coating thickness, which is the threshold value for substrate interference in coating's hardness [26]. Prior to the indentations the foils had been stack on flat glass blocks, with the aid of an extra thin double-faced adhesive tape, to ensure flatness. Each value is the average of 10 measurements.

For adhesion tests the Ni–P–W multilayered coatings were deposited on  $3 \times 1\text{-cm}^2$  copper sheets. The wavelengths of the coatings were 8, 16, 40, 400 and 4000 nm and their average total thickness was 41  $\mu\text{m}$ . The adhesion of the coatings on the copper substrates was studied with the aid of a CSEM REVETEST scratch tester. The scratch tester was equipped with a Rockwell C conical diamond indenter, having a tip angle of  $120^\circ$  and a tip radius of 200  $\mu\text{m}$ . Tests under increasing and constant load were carried out, with the indenter sliding

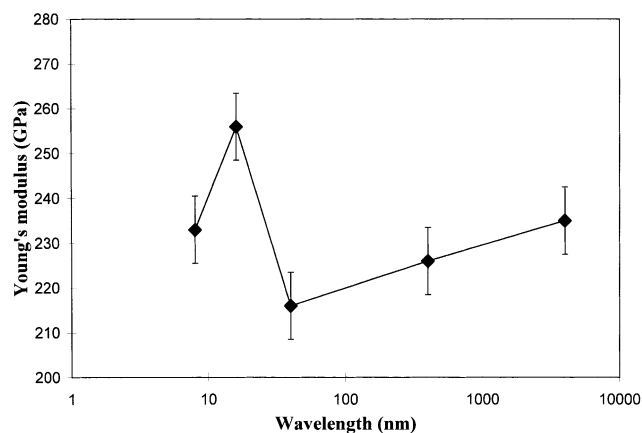


Fig. 1. Young's modulus of the multilayered Ni–P–W coatings vs. wavelength.

speed  $dx/dt$  being 10 mm/min and the loading rate  $dL/dt$  being 100 N/min (for increasing load tests). During the tests, an acoustic emission detector recorded the signals from the specimens, while the scratches were examined with the aid of an optical and a JEOL JSM 6100 scanning electron microscope (SEM). For each set of experimental conditions (increasing and constant load), five tests were carried out and the results given below refer to either average values or representative observations.

### 3. Results and discussion

#### 3.1. Young's modulus

In Fig. 1, the Young's modulus of the multilayered Ni–P–W coatings vs. wavelength is shown. It is seen that for the studied wavelengths no specific trend (increase or decrease), in the modulus values is observed as the wavelength of the coating decreases. On the contrary, the moduli of the amorphous multilayered coatings seem to be dispersed around a mean value of 233 GPa.

The above mean modulus value is higher than the Young's modulus of crystalline nickel (211 GPa [27]) by 10.4%, while the moduli of the coatings are higher than the modulus of crystalline nickel by 2.4–21.3%. It is generally known that amorphous metallic materials produced by the incorporation of a suitable amount of metalloid in the metal matrix, exhibit lower Young's modulus compared with the crystalline state of the metal of the matrix [28]. However, the presence of another metal (tungsten) in the nickel matrix, which has a high Young's modulus (400 GPa [29]) and also reduces the amount of metalloid needed for amorphisation of the layers of the coatings (5 and 8% in weight P instead of 11.6–13% [30,31] for Ni–P amorphous metals), proba

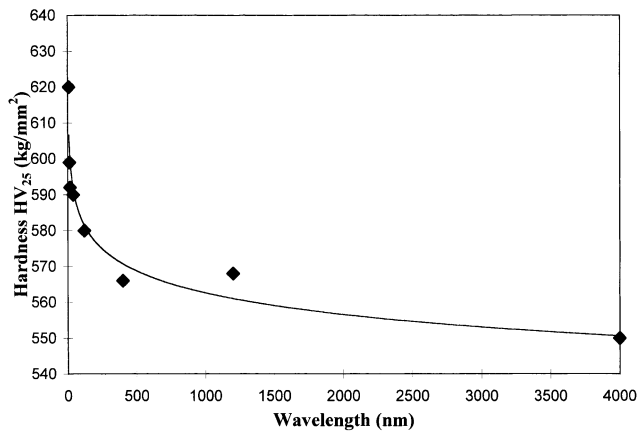


Fig. 2. Microhardness of the multilayered Ni-P-W coatings vs. wavelength.

bly leads to the observed slight increase of the Young's modulus of the multilayered Ni-P-W coatings.

### 3.2. Hardness

In Fig. 2, the microhardness vs. wavelength is shown, for the studied wavelengths of the Ni-P-W multilayered coatings. The solid line is a guide to the eye. A gradual increase in hardness is observed with decreasing wavelength of the coatings. The increase in hardness is more pronounced for wavelengths below 120 nm, while for larger wavelengths the hardness seems to stabilise.

The hardness behaviour of the amorphous Ni-P-W multilayered coatings is similar with the hardness behaviour of multilayers consisting of crystalline layers. In crystalline multilayers, the maximum hardness value in the wavelength range of 2–5 nm is at least 30% higher than the value at large wavelengths, and even higher than the rule of mixtures hardness, estimated using the hardness of the elements consisting the multilayer. In the present study, the maximum hardness value obtained at the smallest wavelength of 8 nm is 13% higher than the hardness value at larger wavelengths. However, hardness shows an intense increase at small wavelengths, and even higher hardness values may be anticipated at wavelengths in the range of 2–5 nm, where its maxima have been observed.

The increase in hardness with decreasing wavelength cannot be described by the theory of Hall-Petch, since it applies to crystalline materials where plastic deformation takes place by dislocation movement.

In amorphous materials, the controlling step for plastic deformation is the initiation of plastic flow. Thus, stresses close to the cohesive strength of these materials are required and as a result, brittle fracture is always competitive to plastic flow. In amorphous ceramics, the strong restriction that covalent bonding imposes on atom movements, causes brittle fracture without any signs of

plastic deformation, while in amorphous metallic materials, the nature of metallic bonding allows a limited amount of plastic deformation to take place before fracture [32].

Plastic flow in amorphous metallic materials is not homogeneous. It takes place by shear transformations, in certain favourable areas in the material. A fraction of atoms in an amorphous metal have a lower co-ordination number than the number dictated by the dense random packing of atoms. Thus, the average atomic volume is larger than expected. This surplus of atomic volume is not uniformly distributed in the amorphous structure, but it is concentrated in isolated areas in the material, forming the free volume areas, which are favourable areas for plastic flow to initiate. For high stresses, coalescence of the shear transformations in the initially isolated free volume areas, leads to the formation of shear bands and generalised plastic deformation of the amorphous metal [33].

Free volume areas have a size distribution which is related with a corresponding activation energy (or stress) distribution, for initiation of plastic flow to take place. It has been shown that large free volume areas require a low activation energy (or stress), while small free volume areas require a high activation energy (or stress) [34].

For small wavelengths, the size of free volume areas is restricted by the layer thickness (especially in the thinner low-W layers), resulting in a distribution of small free volume areas. For large wavelengths, the size of free volume areas is occasionally restricted (or not restricted at all) by the layer thickness, resulting in a distribution of larger free volume areas.

According to the above discussion, when a stress is applied to a Ni-P-W multilayered coating with a large wavelength, a larger fraction of free volume areas are activated, plastic flow is facilitated and thus, hardness is lower. In the case of a Ni-P-W multilayered coating with a small wavelength, the same stress activates a smaller fraction of free volume areas, leading to increased resistance in plastic flow and thus higher hardness.

Argon and Shi [35] estimated the volume of an average free volume area for a Pd<sub>80</sub>Si<sub>20</sub> amorphous metallic alloy (which is an alloy of the metal-metalloid type, similar to our case) to be 0.78 nm<sup>3</sup>. If the free volume area is considered to be of spherical shape, the above value yields a diameter of 1.14 nm. This value shows that layer thickness of low-W layers in Ni-P-W multilayered coatings with small wavelengths (where the increase in hardness is observed), is comparable in size with the free volume areas, thus being capable of affecting their size distribution.

The above mechanism may be responsible for the observed increase in hardness in the multilayered coatings with the smaller wavelengths (i.e. 8, 12 and 16

nm, where the low-W layers are 2, 3 and 4 nm thick, respectively), but it is not expected to be effective for intermediate wavelengths (40 and 120 nm), where a less pronounced increase in hardness is observed.

TEM images of cross-sections of the multilayered coatings showed that for coatings with wavelength of 40 nm and larger, despite the generally amorphous nature of the layers in the multilayered coatings, small crystalline grains  $\sim 5$  nm in diameter can be seen in the low-W layers, adjacent to the interface with the previous high-W layer. It is observed that the small crystalline grains only form at the side of the low-W layers, which follow a high-W layer. The opposite is not observed (more details in reference Panagopoulos et al. [25]). These small crystallites are believed to have high plastic resistances acting as rigid filler in the amorphous phase, thus leading to increased hardness [36]. The effect of the crystallites is stronger in the coatings with the intermediate wavelengths due to the higher number of interfaces in their structure, leading to the slight increase in hardness, whereas for larger wavelengths, the smaller number of interfaces results in a low volume fraction of the crystallites in the structure, rendering them rather incapable of affecting the hardness of the coatings which seems to stabilise.

### 3.3. Adhesion

For the description of the integrity and adhesion of a relatively brittle coating during the scratch test, two characteristic loads are used in literature [23,37]. The first load is the load where the first cracks appear on the coating. It is called cohesive load  $L_c$  and is a measure of the cohesive (intrinsic) strength of the coating. The second load is the minimum load that is required for detachment of the coating from the substrate. It is a measure of the adhesive strength of the coating and it is called adhesive load  $L_A$ . For brittle materials, the adhesive load is usually higher than the cohesive load.

The above loads are identified with the aid of the acoustic emission pattern that is produced during the scratch test. The identification of adhesive load is based on the corresponding sharp increase in the acoustic signal, in case of coating detachment [37,38]. The cohesive load coincides with the load where an acoustic signal is observed for the first time. Examination of the scratch in the optical microscope is very helpful for the identification of cohesive load, since at this load, the first crack can be observed on the surface of the coating, while optical examination can also confirm the detachment of a coating from the substrate. However, it must always be born in mind that the detachment of a coating from its substrate is not necessarily accompanied by a removal of the coating.

In Fig. 3 a–e, representative acoustic emission diagrams of each of the Ni–P–W multilayered alloy coatings, under increasing load from 0 to 80 N are shown. The cohesive load  $L_c$  can be easily identified with accuracy. Its optical identification (with the aid of optical and electron microscopy), yields values between 6 and 13 N for the studied Ni–P–W multilayered coatings. The above values of  $L_c$  are in agreement with the values that are obtained from the acoustic emission patterns (i.e. Fig. 3a–e), given in Table 1.

From the shape of the diagrams in Fig. 3a–e, it is seen that the accurate identification of an adhesive load, for which coating detachment takes place, is not possible. Between 25 and 30 N, a general increase in the acoustic emission level is observed, but this rise cannot be safely attributed to coating detachment alone, since coating thickness, coating and substrate strength, and fracture toughness are important material parameters in the scratch test. The combination of a relatively brittle coating with a ductile substrate (copper), is expected to lead to smaller areas of coating detachment and to a larger number of failure events, producing less intense acoustic signals and thus complicating the acoustic emission patterns. Furthermore, the large coating thickness (approx. 41  $\mu\text{m}$ ), in combination with their brittleness, will lead to the formation of large through-thickness cracks with intense acoustic signals, further complicating the acoustic emission patterns [39].

In an effort to define at least a critical load range (instead of a single load), where loss of coating adhesion seems to take place, observation of the scratch tracks produced under constant (loads of 15, 30, 50, 75 and 100 N) and increasing load (loads 0–80 N) has taken place, with the aid of the optical and electron microscopes. In tracks produced under the action of a constant load and up to a load of 50 N, only narrow cracks are observed on the surface of the coating, which do not lead to substrate exposure. At 75 N, a crack network has been formed in the coatings. Many cracks are wide, leading to substrate exposure through them, while small areas of coating detachment are observed for the first time. At 100 N, cracking of the coating is more intense, while few small areas of coating detachment are also observed. Thus a critical load range for coating detachment seems to exist for loads 50–75 N. It must be noted, however, that even at the highest load, the coating basically remains on the substrate.

In a scratch test, apart from the identification of  $L_A$  and  $L_c$ , the study of the deformation behaviour of the coating–substrate system under the tangential movement of a load acting on the surface of the coating and the investigation of the failure modes of the coating due to the movement of the indenter is also important, since the mode of coating failure may determine its behaviour in a certain application.

The presence of the relatively high acoustic emission level over the whole range of applied normal loads in the scratches under increasing load, which complicates the identification of  $L_A$ , is probably an indication of the compression of the hard coating into the soft substrate [40]. The compressed coating produces an appreciable acoustic signal by further cracking, even after its detachment from the substrate, as it is compressed into the substrate by the action of the moving stylus. Observation of the scratch tracks by the optical microscope, confirmed the existence of the major part of the coatings on the substrate at higher loads, although the coatings were heavily cracked. Any occasional layer detachments along the inner interfaces of the multilayered coatings,

Table 1

Values of cohesive load obtained by acoustic emission patterns

Coating wavelength (nm)	Cohesive load $L_c$ (N)
8	16
16	14
40	9
400	13
4000	5

which are also observed for loads above 30 N, further complicate the shape of the acoustic emission diagrams.

The stepwise increase of acoustic emission signals in the acoustic emission patterns as the load increases and

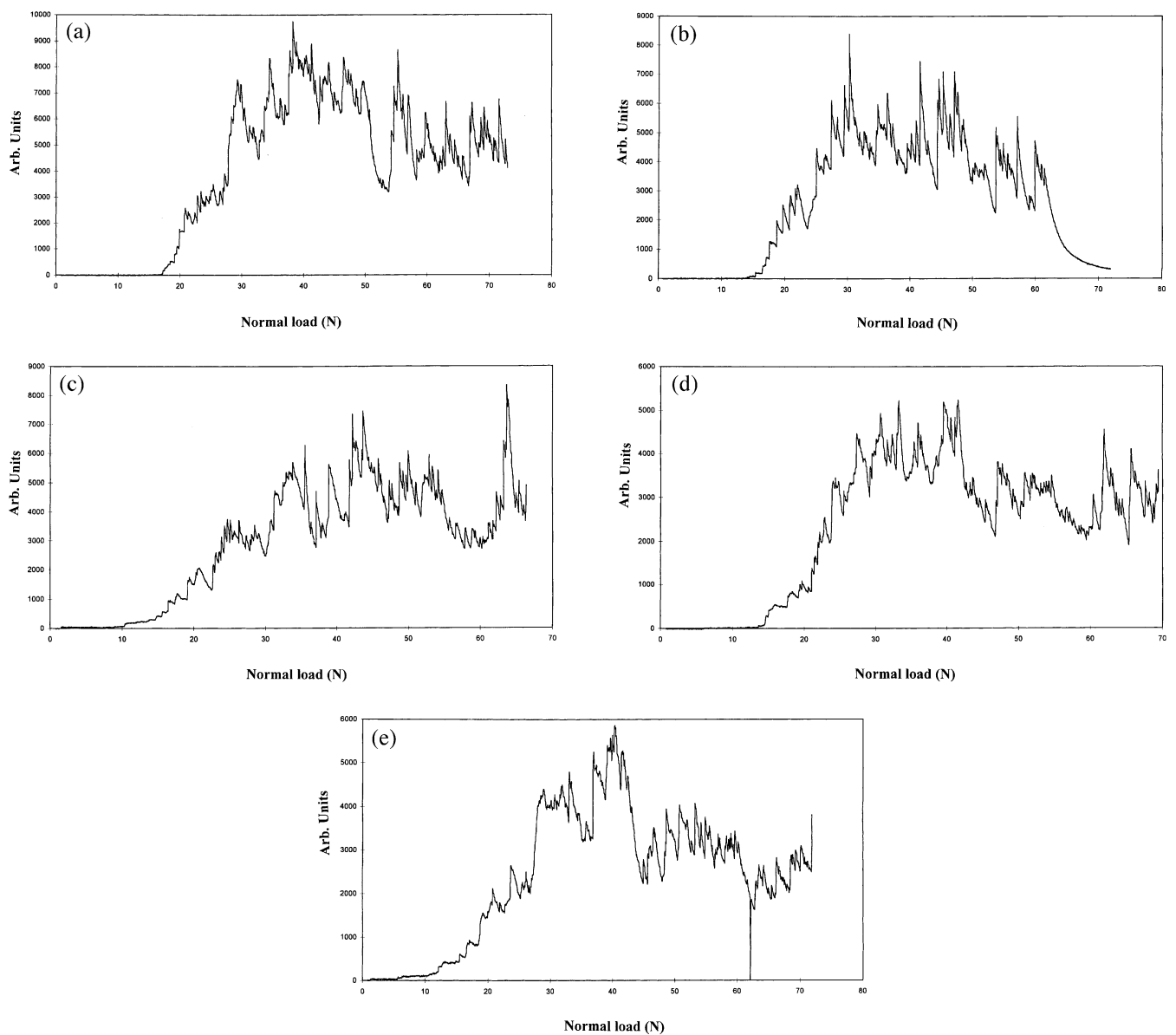


Fig. 3. Acoustic emission diagrams of the Ni-P-W multilayered alloy coatings, under increasing load from 0 to 80 N and for the different wavelengths studied: (a) 8 nm, (b) 16 nm, (c) 40 nm, (d) 400 nm and (e) 4000 nm.

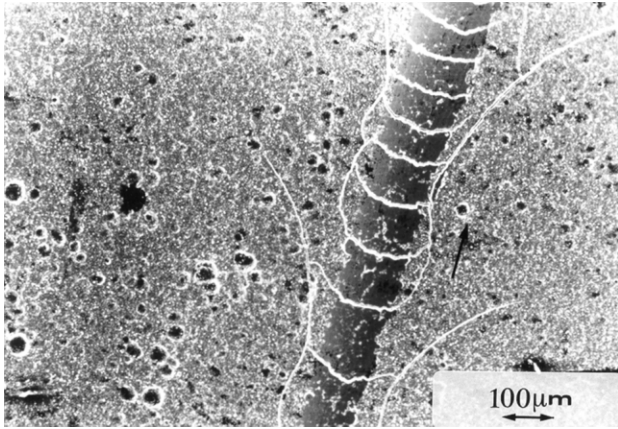


Fig. 4. Scratch morphology under increasing load. Cracks concave to the sliding direction of the indenter are observed, as well as a few lateral cracks at the beginning of the scratch. The load at the shown area is 15 N, the wavelength of the coating is 16 nm. The arrow shows the direction of sliding.

before detachment of the coating takes place (Fig. 3a–e), may be attributed to the gradual propagation of cracks in the coatings, with increasing load. The cracks which form at low loads cannot lead to coating detachment. When they come across an internal interface in the multilayered coating, they either stop or propagate for some distance producing an acoustic signal. As the load increases, new cracks form, which propagate for longer distances across the thickness of the coating or along an internal interface, producing a larger acoustic signal, thus creating the next step of higher acoustic intensity. The old cracks may also expand under the action of higher load, contributing to the acoustic signal. By this way, steps of increasing acoustic intensity are formed with increasing load, in the acoustic emission patterns of the multilayered Ni–P–W coatings.

From the above discussion, it is shown that the adhesion of the multilayered Ni–P–W coatings on copper substrates, is not determined by their wavelength. The results shown in Table 1 might show a dependence of their cohesive strength on wavelength (increase of  $L_c$  for small wavelengths), however, the most significant effect of the layered structure of the coatings seems to be in the shape of the acoustic emission patterns at loads lower than the adhesion load  $L_A$ . The effect of layering in crack propagation may be very advantageous, since the deflection of cracks in the internal interfaces of the multilayered coating, can increase the toughness of the coating significantly.

The failure modes observed in the scratch tests of the Ni–P–W multilayered coatings are common in every coating and seem to depend on the load applied by the indenter. During the scratch tests under the action of increasing load, a sequence of failure modes are observed as the load increases beyond the cohesive load  $L_c$ .

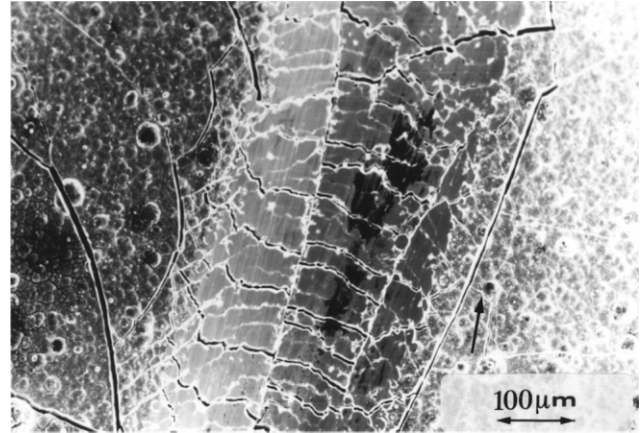


Fig. 5. Morphology of the scratch for a 38-N applied load (test under increasing load). The wavelength of the coating is 4000 nm. The arrow shows the direction of sliding.

For loads slightly higher than the cohesive load (15–25 N), cracks concave to the sliding direction of the indenter are observed (Fig. 4). A small number of cracks which originate from the concave cracks are also observed, which extend outside the scratches, nearly parallel to the direction of sliding. Almost in the middle of scratches (38 N), the concave cracks seem to be deeper, whereas their density has increased. At the sides of the scratch, a network of small and large lateral cracks has been formed (Fig. 5). As the load is further increased (45 N), both concave and convex cracks are observed in the scratches (Fig. 6). Extension of the two above types of cracks outside the scratches, leads to the formation of a network of arc-shaped cracks. Towards the end of the scratches, extensive cracking of the coating is observed. A crack network is formed inside the scratches (Fig. 7), whereas the convex cracks predominate (Fig. 8).

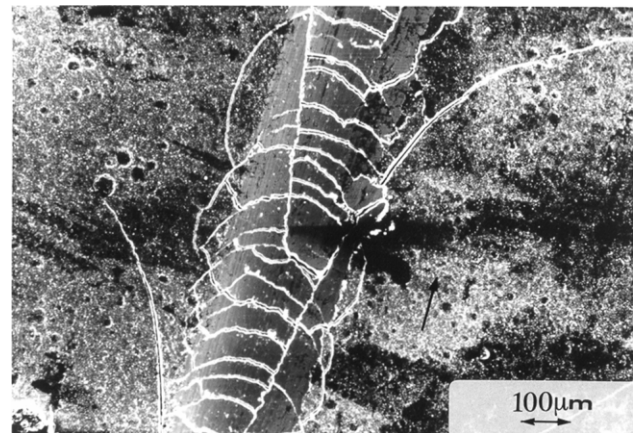


Fig. 6. Morphology of the scratch for a 45-N applied load (test under increasing load). Appearance of the first convex cracks. The wavelength of the coating is 16 nm. The arrow shows the direction of sliding.

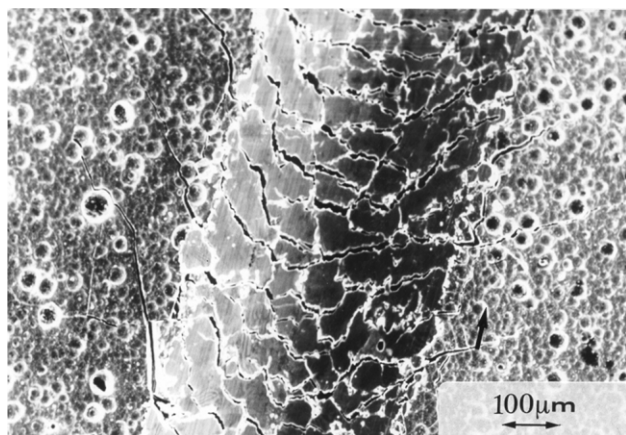


Fig. 7. Morphology of the scratch for a 70-N applied load (test under increasing load). Crack network inside the scratches. The wavelength of the coating is 4000 nm. The arrow shows the direction of sliding.

During increasing load scratch tests, grooves are formed on the surface of the specimens, due to the ductile nature of the copper substrate. At low loads where substrate deformation and depth of the grooves are small, the predominant stresses are tensile stresses generated at the rear of the indenter due to sliding. The tensile stresses are responsible for the formation of concave cracks which predominate for loads up to approximately 35 N. As the load increases, both depth of grooves and substrate deformation increase. The load on the indenter is transferred to its front half, while material is piling-up ahead and to the sides of the indenter. Bending of the coating will set it under tensile stresses at these areas, while the forward movement of the indenter adds compressive stresses to the material ahead, which can lead to buckling. Due to the above actions, at higher loads lateral cracks are formed at the sides of the indenter, parallel to the sliding direction,

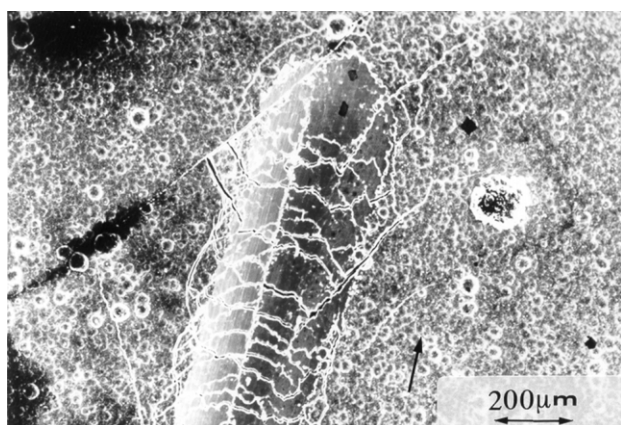


Fig. 8. Morphology of the scratch for a 75–80-N applied load (test under increasing load). Convex cracks and a crack network. The wavelength of the coating is 8 nm. The arrow shows the direction of sliding.

along with convex cracks at the front of the indenter, producing a failure mode known as conformal cracking [39], which is observed in Figs. 6 and 8.

#### 4. Conclusions

In this investigation the effect of layering on Young's modulus, hardness and scratch adhesion of Ni–P–W multilayered alloy coatings was studied and the conclusions were the following:

- The Young's moduli of the amorphous multilayered Ni–P–W coatings studied are higher than the Young's modulus of crystalline nickel. They range from 216 to 256 GPa, while the Young's modulus of crystalline nickel is 211 GPa.
- The hardness of the multilayered Ni–P–W coatings was found to increase with decreasing wavelength of the coatings. The increase in hardness is more pronounced for wavelengths below 120 nm, while for larger wavelengths the hardness seems to stabilise.
- The behaviour of hardness is not interpreted by the Hall–Petch theory, but considering the basic principles of plastic flow in amorphous metallic alloys.
- The cohesive load of the multilayered coatings ranges from 5 to 16 N, as measured by acoustic emission patterns and optical examination of scratches produced under increasing load, while optical observation of the scratch tracks allows the definition of a critical load range of 50–75 N for loss of coating adhesion.
- The values of adhesive loads seem to be independent from the wavelength of the Ni–P–W coatings, while the layered structure seems to affect the shape of the acoustic emission patterns at low loads.
- The failure modes of the Ni–P–W multilayered coatings are common in every coating in the scratch tests under increasing load, and they are a result of substrate deformation and coating brittleness.

#### Acknowledgements

The authors wish to thank Dr K. Stourmaras, President of CERECO for the provision of the scratch tester used in this study. During this research, one of the authors (V.D. Papachristos) was funded by the Greek Foundation for Scholarships.

#### Appendix A:

The bending modulus (or flexural rigidity) of a material ( $D$ ) is given by the following Eq. (A.1) [41]:

$$D = E * I = E * \int_A y^2 dA \quad (\text{A.1})$$

where  $I$  is the material's moment of inertia in respect to

the neutral axis (NA), of its cross-section,  $A$  is the surface of its cross-section and  $y$  is the distance from the neutral axis.

In the case of a plate of a rectangular cross-section of thickness  $b$  and height  $h$ , the moment of inertia for the plate is [41]:

$$I = \int_{-h/2}^{+h/2} by^2 dy = \frac{bh^3}{12} \quad (\text{A.2})$$

The bending modulus of the plate is:

$$D = E^* \frac{bh^3}{12} \quad (\text{A.3})$$

In the case of a plate consisting of  $n$  different layers, and the thickness of the  $i$ th layer is  $h_i$ , the bending modulus of the composite material is [41]:

$$D = \sum_{i=1}^n \int_{\delta_i - h/2}^{\delta_i + h/2} E^* y^2 b dy = \sum_{i=1}^n E^* b \left[ \frac{h_i^3}{12} + h_i \delta_i^2 \right] \quad (\text{A.4})$$

where  $\delta_i$  is the distance of the neutral axis of the cross-section of the  $i$ th layer from the neutral axis of the cross-section of the composite plate.

The cross-section of the plated Cu substrates consisted from the substrate of thickness  $h_s = 600 \mu\text{m}$  and two multilayered Ni–P–W alloy coatings of equal thickness, on both sides of the substrates, producing a symmetrical cross-section, with an obvious neutral axis. The thickness of the coatings on each side of the substrate  $h_c$  was between 39 and 47. According to Eq. (A.3) the bending modulus of the composite material can be given by the following equation:

$$D_{\text{comp}} = E^*_{\text{comp}} \frac{b(h_s + 2h_c)^3}{12} \quad (\text{A.5})$$

where  $E^*_{\text{comp}}$  is the plane strain modulus of the composite material estimated by the acoustic-wave resonance method.

According to Eq. (A.4) the bending modulus of the composite material can be given by Eq. (A.6):

$$D_{\text{comp}} = 2E^*_c b \left[ \frac{h_c^3}{12} + h_c \left( \frac{h_c + h_s}{2} \right)^2 \right] + E^*_s b \left[ \frac{h_s^3}{12} \right] \quad (\text{A.6})$$

where  $E^*_c$  and  $E^*_s$  are the plane strain moduli of the coating and the substrate (measured by the acoustic-wave resonance method), respectively.

Since Eq. (A.5) = Eq. (A.6),  $E^*_c$  (the plane strain modulus of the multilayered coating) can be estimated.

## References

- [1] W.M.C. Yang, T. Tsakalakos, J.E. Hilliard, J. Appl. Phys. 48 (1977) 876.
- [2] L.R. Testardi, R.H. Willens, J.T. Krause, D.B. McWhan, S. Nakahara, J. Appl. Phys. 52 (1981) 510.
- [3] G.E. Henein, J.E. Hilliard, J. Appl. Phys. 54 (1983) 728.
- [4] T. Tsakalakos, J.E. Hilliard, J. Appl. Phys. 54 (1983) 734.
- [5] D. Baral, J.B. Ketterson, J.E. Hilliard, J. Appl. Phys. 57 (1985) 1076.
- [6] T.B. Wu, J. Appl. Phys. 53 (1982) 5265.
- [7] D. Wolf, J.F. Lutsko, Phys. Rev. Lett. 60 (1988) 1170.
- [8] R.C. Cammarata, K. Sieradzki, Phys. Rev. Lett. 62 (1989) 2005.
- [9] B.M. Davis, D.N. Seidman, A. Moreau, J.B. Ketterson, J. Mattson, M. Grimsditch, Phys. Rev. B 43 (1991) 9304.
- [10] A. Fartash, E.E. Fullerton, I.K. Schuller, S.E. Bobbin, J.W. Wagner, R.C. Cammarata, S. Kumar, M. Grimsditch, Phys. Rev. B 44 (1991) 13760.
- [11] G.W. Tecza, Phys. Rev. B 46 (1992) 15447.
- [12] M.K. Small, B.J. Daniels, B.M. Clemens, W.D. Nix, J. Mater. Res. 9 (1994) 25.
- [13] F.H. Streitz, R.C. Cammarata, K. Sieradzki, Phys. Rev. B 49 (1994) 10707.
- [14] R.C. Cammarata, T.E. Schlensiger, C. Kim, S.B. Qadri, A.S. Edelstein, Appl. Phys. Lett. 56 (1990) 1862.
- [15] I. Toshiya, R. Yamamoto, A. Yoshihara, Surf. Coat. Technol. 45 (1991) 215.
- [16] A.F. Jankowski, J. Magn. Magn. Mater. 126 (1993) 185.
- [17] J.A. Ruud, T.R. Jervis, F. Spaepen, J. Appl. Phys. 75 (1994) 4969.
- [18] C. Kim, S.B. Qadri, M.R. Scanlon, R.C. Cammarata, Thin Solid Films 240 (1994) 52.
- [19] M.R. Scanlon, R.C. Cammarata, D.J. Keavney, J.W. Freeland, J.C. Walker, C. Hayzelden, Appl. Phys. Lett. 66 (1995) 46.
- [20] B.J. Daniels, W.D. Nix, B.M. Clemens, Appl. Phys. Lett. 66 (1995) 2969.
- [21] S. Koehler, Phys. Rev. B 2 (1970) 547.
- [22] T.G. Nieh, J. Wadsworth, Scr. Metall. Mater. 25 (1991) 955.
- [23] F.C. Chang, M. Levy, R. Huie, M. Kane, P. Buckley, T.Z. Kattamis, G.R. Lakshminarayan, Surf. Coat. Technol. 49 (1991) 87.
- [24] K.L. Lin, S.K. Chen, S.Y. Chang, J. Mater. Sci.: Mater. Electron. 8 (1997) 253.
- [25] C.N. Panagopoulos, V.D. Papachristos, U. Wahlstrom, P. Leisner, L.W. Christoffersen, Scr. Mater. 43 (2000) 677.
- [26] H.E. Boyer (Ed.), Hardness Testing, ASM International, Metals Park Ohio, OH, 1987.
- [27] M.F. Ashby, D.R.H. Jones, Engineering Materials 2, Pergamon Press, Oxford, 1986, p. 10.
- [28] Y. Suzuki, T. Egami, J. Non-Cryst. Solids 75 (1985) 361.
- [29] W.D. Callister, Materials Science and Engineering, An Introduction, John Wiley, New York, 1997.
- [30] E. Bredael, B. Blanpain, J.P. Celis, J.R. Roos, J. Electrochem. Soc. 141 (1994) 294.
- [31] G. McMahon, U. Erb, J. Mater. Sci. Lett. 8 (1989) 865.
- [32] A.S. Argon, Inelastic deformation, fracture of glassy solids, in: Plastic Deformation and Fracture of Materials, VCH, 1993, p. 468.
- [33] D. Turnbull, M.H. Cohen, J. Chem. Phys. 52 (1970) 3038.
- [34] A.S. Argon, Inelastic deformation, fracture of glassy solids, in: Plastic Deformation and Fracture of Materials, VCH, 1993, p. 475.
- [35] A.S. Argon, L.T. Shi, Philos. Mag. A46 (1982) 275.
- [36] A.S. Argon, in: H.J. McQueen, J.-P. Bailon, J.I. Dickson, J.J. Jonas, M.G. Akben (Eds.), Strength of Metals and Alloys, vol. 3, Pergamon Press, Oxford, 1986, p. 2007.

- [37] A.R. Chalker, S.J. Bull, D.S. Rickerby, *Mater. Sci. Eng. A* 140 (1991) 583.
- [38] A.J. Perry, *Thin Solid Films* 107 (1983) 167.
- [39] S.J. Bull, *Surf. Coat. Technol.* 50 (1991) 25.
- [40] H. Jensen, U.M. Jensen, G. Sorensen, *Surf. Coat. Technol.* 74–75 (1995) 297.
- [41] L.H. Crandall, N.C. Dahl, T.J. Lardner, *An Introduction to the Mechanics of Solids*, McGraw–Hill, 1978.